Annales Geophysicae, 23, 2385–2390, 2005
SRef-ID: 1432-0576/ag/2005-23-2385

Annales Geophysicae

Relationship between propagation direction of gravity waves in OH and OI airglow images and VHF radar echo occurrence during the SEEK-2 campaign

F. Onoma[1,*], Y. Otsuka[1], K. Shiokawa[1], T. Ogawa[1], M. Yamamoto[2], S. Fukao[2], and S. Saito[3]

[1]Solar-Terrestrial Environment Laboratory, Nagoya University, Honohara 3-13, Toyokawa, Aichi 442-8507, Japan
[2]Research Institute for Sustainable Humanosphere, Kyoto University, Gokasho, Uji, Kyoto 611-0011, Japan
[3]National Inst. of Information and Communications Technology, 4-2-1 Nukui-Kitamachi, Koganei, Tokyo 184-8795, Japan
[*]now at: Mitsubishi Electric Corp., Chiyoda-ku, Tokyo 100-8310, Japan

Received: 14 December 2004 – Revised: 17 May 2005 – Accepted: 1 June 2005 – Published: 13 October 2005

Part of Special Issue "SEEK-2 (Sporadic-*E* Experiment over Kyushu 2)"

Abstract. We report simultaneous observations of atmospheric gravity waves (AGW) in OI (557.7 nm) and OH airglow images and VHF radar backscatter from field-aligned irregularities (FAI) in the *E*-region during the SEEK-2 (Sporadic-*E* Experiment over Kyushu 2) campaign period from 29 July to 9 August 2002. An all-sky imager was operated at Nishino-Omote (30.5° N, 130.1° E), Japan. On 14 nights, 17 AGW events were detected in OI and OH airglow images. AGW propagated mostly toward the northeast or southeast. From comparison with the *E*-region FAI occurrence, which is detected by a nearby VHF radar (31.57 MHz), we found that AGW tended to propagate southeastward during FAI events. This result suggests that the interaction between AGW and *E*-region plasma plays an important role in generating FAI. Furthermore, polarization electric fields generated directly by AGW may contribute to the FAI generation.

Keywords. Atmospheric composition and structure (Airglow and aurora), Ionosphere (Ionospheric irregularities, Mid-latitude ionosphere)

1 Introduction

Detailed structures of field-aligned irregularities (FAI) in the nighttime mid-latitude *E*-region were first investigated with the powerful middle and upper atmosphere (MU) radar at Shigaraki, Japan (34.9° N, 136.1° E) by Yamamoto et al. (1991), who found two types of radar echoes: "quasi-periodic" echoes (QP echoes) and "continuous" echoes. The continuous echoes appear continuously in time at an altitude of 90–100 km, mainly around sunrise and occasionally at night (Ogawa et al., 1995). The QP echoes appear intermittently at an altitude around 100 km, with periods of 5–20 min during the post-sunset period. On a range-time-intensity (RTI) plot, the QP echoes have striations with positive or negative slope. The morphological features of the QP echoes were clarified by Yamamoto et al. (1992). Yamamoto et al. (1994) conducted multibeam (12 directions) observations with the MU radar and found that the QP echo region has a monochromatic wave structure that propagates toward the southwest with a wavefront elongating from NW to SE and a typical wavelength of 5–15 km. These QP echo features suggest that the generation of the QP echoes is associated with the existence of atmospheric gravity waves (AGW) (e.g. Woodman et al., 1991; Tsunoda et al., 1994; Ogawa et al., 1995).

With the advent of an airglow imaging technique using a CCD camera, two-dimensional structures of airglow perturbations at the mesopause region caused by AGW have been studied since the 1990s. The first SEEK (Sporadic-E Experiment over Kyushu) campaign was carried out in August, 1996. Nakamura et al. (1998) and Taylor et al. (1998) have reported the characteristics of the AGW observed in OH and OI(557.7 nm) airglow images at Shigaraki, and Yamagawa, Japan during the campaign period. Although *E*-region FAI were observed by VHF radar (Tsunoda et al., 1998; Yamamoto et al., 1998), no comparison between the characteristics of AGW and FAI occurrences was made. In this paper, we investigate, for the first time, relationships between the propagation direction of AGW in airglow images and the FAI occurrence observed simultaneously with a 31.57-MHz VHF radar.

Correspondence to: F. Onoma
(onoma@stelab.nagoya-u.ac.jp)

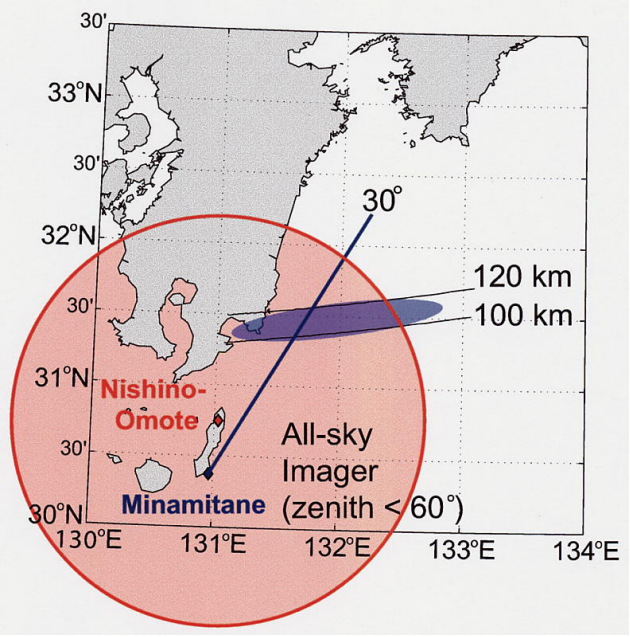

Fig. 1. Map showing location of the all-sky imager (Nishino-Omote) and VHF radar (Minamitane). Field-of-view of the all-sky imager with zenith angle less than 60°is shown by a circle (radius of 160 km). Area observed with the VHF radar is also shown by the shaded area in the figure.

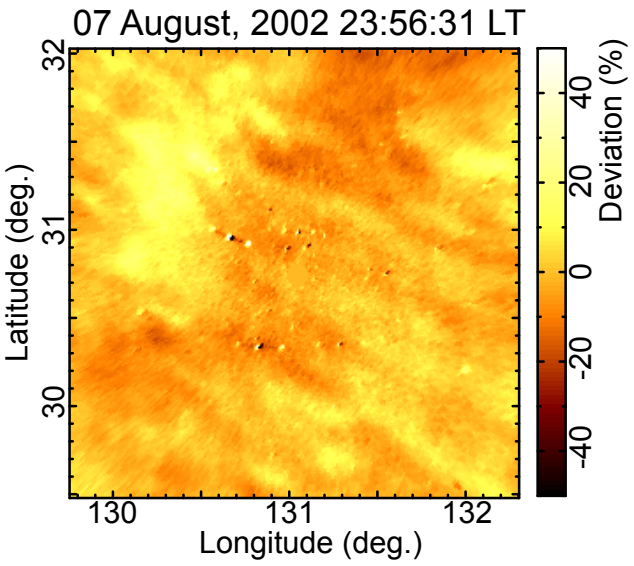

Fig. 2. Two-dimensional map of OI (557.7 nm) airglow perturbation in the geographical coordinate.

2 Observations

An all-sky airglow imager was operated at Nishino-Omote (30.5° N, 131.1° E), Japan during the SEEK-2 campaign period from 27 July to 9 August 2002. This imager had five optical filters, a fish-eye lens with a field-of-view (FOV) of 180°, and a cooled-CCD camera with 512×512 pixels. Details of the imager system were described by Shiokawa et al. (1999). Two-dimensional images of OI (557.7 nm) and OH-band (790–910 nm) airglow intensity were obtained every 330 s, with exposure times of 145 s and 15 s, respectively. Figure 1 shows the location and FOV of the imager (60°off-zenith).

The Lower Thermosphere Profiler Radar (LTPR), a VHF backscatter radar at 31.57 MHz with a peak power of 20 kW, was operated at Minamitane (30.4° N, 131.0° E), Japan during a period from 30 July to 24 August 2002. Details of the radar system and observational mode are described by Saito et al. (2005). The radar beam was pointed to the northeast (azimuth of 30°). Perpendicularity of the beam to the geomagnetic field line at an altitude of around 100 km was achieved at a zenith angle of 53°. *E*-region FAI echoes were expected to be observed at altitudes between 100 and 120 km (e.g. Yamamoto et al., 1992). The altitudes of FAI echoes can be determined by interferometry technique (Saito et al., 2005). Locations where the radar beam directions are perpendicular to the geomagnetic fields at 100 and 120 km altitudes are shown by a solid curve in Fig. 1. Since the FAI region probed by the LTPR was within the imager FOV, this setup allowed us to investigate the relationship between FAI and AGW.

3 Results

During 27 July–9 August 2002, 702 (831) images of the OI (OH) airglow were obtained. Of these, 397 OI and 472 OH images were obtained under clear sky conditions. Figure 2 shows an example of an OI airglow image. The original all-sky image was mapped into geographical coordinates, assuming that the OI airglow layer exists at an altitude of 96 km. The OH airglow layer is assumed to exist at an altitude of 86 km. A median-filter was applied to the image to remove stars. To see perturbations of the airglow intensity clearly, the percentage of airglow intensity deviations to the background (from 1-h average) is shown in the image with a pseudo-color scale of ±50%. The minimum amplitude of waves detected by this method is estimated to be about 5%. In the image, wavy structures of the airglow intensity can be seen. The wavefronts of the structure elongate from NW to SE. The horizontal wavelength and phase velocity are 16 km and 30 m/s, respectively.

To investigate statistically the occurrence rate and propagation characteristics of the wavy structures, all the observation periods were divided into 1-h bins. The occurrence rate of AGW was defined as the ratio of the number of bins containing AGW patterns to the number of bins under clear sky conditions. The occurrence rates in OI and OH images were 65% and 83%, respectively.

By analyzing successive images, 17 AGW events in total were obtained on 14 nights under clear sky. On each event, the horizontal wavelength, horizontal propagation direction, and period of AGW were determined. These wave

Table 1. Summary of wave events detected at Nishino-Omote for eight nights. V_p and λ_h indicate horizontal phase velocity and horizontal wavelength of gravity wave, respectively. α indicates the azimuth (clockwise from geographic north) of gravity wave propagation. Local time is UT+9 h.

Date (UT)	Time (UT)	Emission	V_p (m/s)	λ_h (km)	α (deg.)
1 August	11:29	OH	31.4	18.9	30
	11:30	OI	27.3	43.0	45
	13:41	OI	44.0	43.5	24
2 August	12:05	OH	24.4	13.5	135
	12:05	OI	72.2	29.8	−129
3 August	15:11	OI	18.7	33.0	30
4 August	12:52	OI	63.9	20.2	135
	13:28	OH	45.0	17.2	127
	16:05	OI	27.7	10.6	127
5 August	15:35	OI	59.7	80.0	34
	15:58	OH	17.9	30.5	37
6 August	11:41	OI	37.5	20.2	135
	13:26	OH	39.6	62.5	125
	17:46	OI	28.9	11.7	125
7 August	14:52	OI	29.9	15.6	35
	16:10	OH	34.2	31.2	35

Table 2. Summary of occurrence rate of E-region field-aligned irregularities (FAI). Each number indicates the count of bin (10 min) during which FAI occurred. – indicates a lack of data. Local time is UT+9 h.

Date (UT)	10	11	12	13	14	15	16	17	18	19	20
30 July	0	0	0	0	0	0	0	0	0	0	0
31 July	0	0	1	0	0	0	0	0	0	0	0
1 August	0	1	1	0	1	0	0	0	0	0	0
2 August	1	0	1	0	0	0	0	0	0	0	0
3 August	–	–	–	1	6	2	0	0	0	0	0
4 August	2	6	6	6	6	6	4	6	3	0	0
5 August	–	–	–	–	–	–	–	–	–	–	–
6 August	0	1	0	0	3	6	6	4	5	1	3
7 August	4	4	5	1	0	0	0	0	0	0	0
8 August	3	6	5	6	0	0	0	0	0	0	0
9 August	3	3	6	6	6	5	0	2	5	0	0

parameters are listed in Table 1. The horizontal wavelengths range from 10 to 90 km and most of them are 10–50 km in both airglow images. The horizontal phase velocities distribute from 10 to 80 m/s with an average of 37 m/s.

During the airglow observation periods, LTPR was operated to observe backscatter from FAI in the E-region. During 19:00–21:00 LT on 3 August and 19:00–29:00 LT on 5 August, data were not obtained due to instrumental problems. The LTPR observation period were divided into bins with 10 minutes. FAI echo occurrence was defined when the echo intensity was greater than 0 dB in each 10-min bin. The FAI occurrence rates are listed in Table 2. The FAI echoes were detected on 9 of 10 nights. Only on the night of 30 July, did the FAI echo not appear. The occurrence rate of the FAI echo is higher before midnight than after midnight. This tendency is consistent with previous observations using MU radar at Shigaraki, Japan (34.9° N, 136.1° E) (Yamamoto et al., 1992).

Figure 3 shows the distribution of azimuths of the AGW in OI and OH images. The radial scale indicates the number of AGW events in each direction. All the AGW events are divided into two cases; one is the case in which E-region FAI echoes were detected in more than 3 bins in one hour with LTPR (Fig. 3a), and the other is the case without the FAI echoes (Fig. 3b). Figure 3 shows a clear difference in the propagation directions of AGW between both cases. In the case with FAI, most of AGW in both airglow images propagate southeastward. In the case without FAI, on the contrary, AGW in OI prefer northeastward propagation. For OH, AGW have two distinct preferences of propagation direction (northeastward and southeastward).

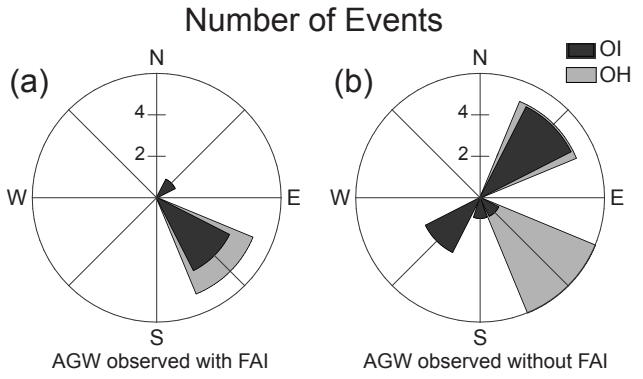

Fig. 3. Azimuthal distribution of AGW propagation direction observed at Nishino-Omote, Japan. All events were categorized into two types: **(a)** AGW simultaneously observed with FAI, **(b)** AGW observed without FAI.

4 Discussion

In the present study, 17 events of AGW were obtained in OI and OH airglow images at Nishino-Omote during the SEEK-2 campaign. During the SEEK-1 campaign (17–22 August 1996), an all-sky airglow imager was installed at Yamagawa, 87 km northwest from Nishino-Omote. Taylor et al. (1998) reported that 14 events of wave structure were detected successfully for five nights in clear-sky conditions. Horizontal wavelength and horizontal wave velocity of the AGW during the SEEK-2 campaign are consistent with the previous observation during the SEEK-1 campaign.

As for the azimuth of AGW in OI and OH images, most AGW during SEEK-1 and SEEK-2 have an eastward component in their propagation direction. This is consistent with the results obtained from a statistical study of AGW in mesospheric airglow images at Shigaraki and Rikubetsu, Japan (Nakamura et al., 1999, 2001; Ejiri et al., 2003). AGW propagating upward are absorbed by the background wind when the phase velocity of AGW reaches the background wind velocity (critical level) (Bretherton, 1966). At mid-latitudes, the zonal wind in the mesosphere (50–80 km) in summer blows strongly westward. This strong wind filters out AGW that propagate westward, and only the AGW that have an eastward component of the propagation can propagate upward beyond 80 km.

From the comparison between E-region FAI and AGW seen in OI and OH airglow images, we have shown that a meridional component of the AGW propagation direction tends to be related to FAI occurrence. In the case when the propagation direction of AGW had a southward component, FAI were frequently observed. On the other hand, in the case when the propagation direction had a northward component, FAI did not appear. It is known that FAI propagate southwestward (e.g. Yamamoto et al., 1997). During the SEEK-2 campaign, striated FAI echoes had a negative slope on the range-time-intensity (RTI) plot, indicating that FAI movement had a southward (toward the radar) component (Saito et al., 2005).

FAI are expected to move by $\mathbf{E}\times\mathbf{B}$ drift or neutral winds with the same velocity as the ambient plasma in the E_s layer. The E_s layer is formed by the vertical shear in zonal wind which is eastward below the E_s layer and westward above the E_s layer (Whitehead, 1961). Larsen et al. (1998) have observed neutral winds exceeding 120 m/s at around the E_s layer altitude in Japan during the Sporadic-E Experiment over Kyushu (SEEK) campaign in 1996. Since the wind velocity would be larger than $\mathbf{E}\times\mathbf{B}$ drift velocity, on average, movement of the plasma in the E_s layer would be mainly controlled by the neutral winds. The wind would rotate with increasing altitude, as expected from tidal theory. Therefore, the neutral wind would blow southward at the altitude of the E_s layer. The plasma in the E_s layer is expected to move southward with almost the same velocity as the neutral wind because of high ion-neutral collision frequency. Therefore, the observational results in the present study suggest that AGW propagating toward the same direction as the plasma in the E_s layer play an important role in generating FAI.

Due to AGW, the neutral particles oscillate in a direction perpendicular to the wave propagation direction. Ions in the E_s layer move at the same velocity as neutral particles due to collision with neutral particles. Under the condition that the AGW and background plasma motion have the same component in the propagation direction, the interaction time between the neutral particles and ions is prolonged. This concept of increasing interaction time by matching velocities is called the spatial resonance (Whitehead, 1971). Under the condition that the spatial resonance takes place, plasma structure in the E_s layer is largely modulated and spatial variations of the plasma density in the E_s layer would be generated. Background electric current and spatial variation of plasma density in the E_s layer generate polarization electric fields to keep continuity of the electric current. Maruyama et al. (2000) have proposed a mechanism for producing altitude-extended QP striations (see also Ogawa et al., 2002). In their model, polarization electric fields are generated from a high-density plasma cloud within the E_s layer and mapped upward along the geomagnetic field with a little attenuation. These electric fields drive ions in the background E-region and produce field-aligned plasma structures. These plasma structure and polarization electric fields generate the gradient-drift instability causing FAI. However, the mechanism to produce a localized enhancement of the plasma density has not been revealed. Our results suggest that AGW plays an important role in producing the plasma density enhancement.

Using a three-dimensional simulation model that can simulate generation of polarization electric fields due to the inhomogeneity of plasma density, Yokoyama et al. (2004) have shown that southward propagating AGW are more effective in generating polarization electric fields than northward propagating AGW. The explanation of this feature is as follows. Neutral particle motion due to AGW across the geomagnetic field generates polarization electric fields because of the difference between ion and electron motions. Direction of the polarization electric fields are variable according

to the phase of neutral particle oscillation due to AGW. In the case of northward propagating AGW, different phases of the polarization electric fields are penetrated by the same geomagnetic field line because the wave front of AGW is nearly perpendicular to the geomagnetic field. They cancel each other out along the geomagnetic field. On the other hand, the polarization electric fields generated by southward propagating AGW are not easily canceled. Since the polarization electric fields would be mapped along the geomagnetic field and cause gradient drift instability, southward propagating AGW are preferable for FAI occurrence. Our observational results support this idea.

5 Conclusions

During the SEEK-2 campaign period from 27 July to 9 August 2002, we observed AGW at altitudes of 86 km and 96 km in OI and OH-band airglow images. Wave parameters of the observed AGW are consistent with previous observation during the SEEK-1 campaign. LTPR at 31.57 MHz was operated during this period to observe field-aligned irregularities (FAI) in the E-region. Comparison between propagation directions of AGW and FAI occurrence shows that AGW during FAI events have a tendency to propagate southeastward. AGW would modulate the E_s layer. In the modulated E_s layer, the background electric current would generate polarization electric fields to keep the electric current continuity. The generated polarization electric fields map along the geomagnetic field to the higher E region and from field-aligned plasma density structures. These plasma structure and polarization electric fields would generate the gradient-drift instability causing FAI. The present study suggests that the spatial resonance of southeastward propagating AGW with E-region plasma may contribute to the generation of FAI. Furthermore, polarization electric fields generated directly by AGW with southward phase velocity may play an important role in the generation of FAI.

Acknowledgements. We thank Y. Katoh, M. Satoh, T. Katoh, S. Suzuki, and N. Kotake of the Solar-Terrestrial Environment Laboratory, Nagoya University, for kind support to airglow imaging observations. The LTPR was owned and operated by the Research Institute for Sustainable Humanosphere of Kyoto University. Authors are grateful to Nishino-Omote city, Kagoshima prefecture, Japan and Japanese Aerospace Exploration Agency for their kind support to the airglow and radar observations. This work was supported by a Grant-in-Aid for Scientific Research of the Ministry of Education, Culture, Sports, Science and Technology of Japan (11440145).

Topical Editor M. Pinnock thanks A. V. Koustov for his help in evaluating this paper.

References

Bretherton, F. P.: Propagation of groups of internal gravity waves in a shear flow: Quart. J. Roy. Meteor. Soc., 92, 466–480, 1966.

Ejiri, M. K., Shiokawa, K., Ogawa, T., Igarashi, K., Nakamura, T., and Tsuda, T.: Statistical study of short-period gravity waves in OH and OI nightglow images at two separated sites, J. Geophys. Res., 108(D21), 4679, doi:10.1029/2002JD002795, 2003.

Larsen, M. F., Fukao, S., Yamamoto, M., Tsunoda, R., Igarashi, K., and Ono, T.: The SEEK chemical release experiment: Observed neutral wind profile in a region of sporadic E, Geophys. Res. Lett., 25, 1789–1792, 1998.

Maruyama, T., Fukao, S., and Yamamoto, M: A possible mechanism for echo striation generation of radar backscatter from midlatitude sporadic E, Radio Sci., 35, 1155–1164, 2000.

Nakamura, T., Tsuda, T., Miyagawa, H., and Matsushita, Y.: Propagation directions of gravity wave patterns observed in OH CCD images during the SEEK campaign, Geophys. Res. Lett., 25, 1793–1796, 1998.

Nakamura, T., Higashikawa, A., Tsuda, T., and Matsushita, Y.: Seasonal variations of gravity wave structures in OH airglow with a CCD imager at Shigaraki, Earth Pl. Sp., 51, 897–906, 1999.

Nakamura, T., Tsuda, T., Maekawa, R., Tsutsumi, M., Shiokawa, K., and Ogawa, T.: Seasonal variation of gravity waves with various temporal and horizontal scales in the MLT region observed with radar and airglow imaging, Adv. Space. Res., 27, 1737–1742, 2001.

Ogawa, T., Yamamoto, M., and Fukao, S.: Middle and upper atmosphere radar observations of turbulence and movement of midlatitude sporadic E irregularities, J. Geophys. Res., 100, 12 173–12 188, 1995.

Ogawa, T., Takahashi, O., Otsuka, Y., Nozaki, K., and Kita, K.: Simultaneous middle and upper atmosphere radar and ionospheric sounder observations of midlatitude E region irregularities and sporadic E layer, J. Geophys. Res., 107(A10), 1275, doi:10.1029/2001JA900176, 2002.

Saito, S., Marumoto, M., Yamamoto, M., Fukao, S., and Tsunoda, T.: Radar observations of field-aligned plasma irregularities in the SEEK-2 campaign, Ann. Geophys., 23, 2307–2318, 2005.

Shiokawa, K., Katoh, Y., Satoh, M., Ejiri, M. K., Ogawa, T., Nakamura, T., Tsuda, T., and Wiens, R. H.: Development of optical mesosphere thermosphere imagers (OMTI), Earth Pl. Sp., 51, 887–896, 1999.

Taylor, M. J., Seo, S. H., Nakamura, T., Tsuda, T., Fukunishi, H., and Takahashi, Y.: Long base-line measurements of short-period mesospheric gravity waves during the SEEK campaign, Geophys. Res. Lett., 25, 1797–1800, 1998.

Tsunoda, R. T., Fukao, S., and Yamamoto, M.: On the origin of quasi-periodic radar backscatter from midlatitude sporadic E, Radio Sci., 20, 349–365, 1994.

Tsunoda, R. R., Fukao, S., Yamamoto, M., and Hamasaki, T.: First 24.5-MHz radar measurements of quasi-periodic backscatter from field-aligned irregularities in midlatitude sporadic E, Geophys. Res. Lett., 25, 1765–1768, 1998.

Whitehead, J. D.: The formation of the sporadic-E layer in the temperate zones, J. Atmos. Terr. Phys., 20, 49–58, 1961.

Whitehead, J. D.: Ionization disturbances caused by gravity waves in the presence of an electrostatic field and background wind, J. Geophys. Res., 76, 238–241, 1971.

Woodman, R. F., Yamamoto, M., and Fukao, S.: Gravity wave modulation of gradient drift instabilities in mid-latitude sporadic E irregularities, Geophys. Res. Lett., 18, 1179–1200, 1991.

Yamamoto, M., Fukao, S., Woodman, R. R., Ogawa, T., Tsuda, T., and Kato, S.: Mid-latitude E region field-aligned irregularities observed with the MU radar, J. Geophys. Res., 96, 15 943–15 949, 1991.

Yamamoto, M., Fukao, S., Ogawa, T., Tsuda, T., and Kato, S.: A morphological study on mid-latitude E-region field-aligned ir-

regularities observed with the MU radar, J. Atmos. Terr. Phys., 54, 769–777, 1992.

Yamamoto, M., Komoda, N., Fukao, S., Tsunoda, R. T., Ogawa, T., and Tsuda, T.: Spatial structure of the *E* region field-aligned irregularities revealed by the MU radar, Radio Sci., 29, 337–347, 1994.

Yamamoto, M., Fukao, S., Tsunoda, R. T., Igarashi, K., and Ogawa, T.: Preliminary results from joint measurements of *E*-region field-aligned irregularities using the MU radar and the frequency-agile radar, J. Atmos. Terr. Phys., 59, 1655–1663, 1997.

Yamamoto, M., Itsuki, T., Kishimoto, T., Tsunoda, R. T., Pfaff, R. F., and Fukao, S.: Comparison of E-region electric fields observed with a sounding rocket and a Doppler radar in the SEEK campaign, Geophys. Res. Lett., 25, 1773–1776, 1998.

Yokoyama, T., Horinouchi, T., Yamamoto, M., and Fukao, S.: Modulation of the midlatitude ionospheric *E* region by atmospheric gravity waves through polarization electric field, J. Geophys. Res., 109(A12307), doi:10.1029/2004JA010508, 2004.